Spectrum of Engineering Sciences
ISSN (e) 3007-3138 (p) 3007-312X Volume 3, Issue 8, 2025

FACILE LOW-TEMPERATURE SYNTHESIS OF ANATASE TIO_2 NANOPARTICLES AND THEIR APPLICATION IN NANOCRYSTALLINE THIN FILM FABRICATION

Zia Un Nabi[*1], **Muhammad Abid**[2], **Salman Khan**[3]

[*1,3]*BS Physics Federal Urdu University of Arts, Sciences & Technology*
[2]*University of Malakand Pakistan*

[*1]ziayousafzai3@gmail.com, [2]muhammadabidroghani123@gmail.com

DOI: https://doi.org/10.5281/zenodo.16791942

Keywords
Anatase TiO_2, Low-temperature synthesis, Nanoparticles, Thin film fabrication, Photocatalysis, Sol–gel method

Article History
Received: 27 April, 2025
Accepted: 04 August, 2025
Published: 11 August, 2025

Corresponding Author: *
Zia Un Nabi

Abstract

Titanium dioxide (TiO_2), particularly in its anatase phase, has emerged as a promising material for applications in photocatalysis, photovoltaics, and transparent conducting films due to its high photoactivity, chemical stability, and non-toxicity. However, conventional synthesis routes often require high-temperature processing (>300 °C), which limits the choice of compatible substrates and increases fabrication costs. This study presents a facile, low-temperature synthesis method for producing phase-pure anatase TiO_2 nanoparticles, followed by their integration into nanocrystalline thin films suitable for optoelectronic and energy applications.

The synthesis approach utilizes a modified sol–gel route at sub-100 °C, incorporating chelating agents and pH control to achieve nanoparticle sizes below 20 nm with narrow distribution and excellent dispersibility. Structural analysis via XRD and TEM confirms the dominance of the anatase phase, while FTIR and UV–Vis spectroscopy reveal functional group coordination and strong optical absorption. Thin films were fabricated through spin-coating and annealed below 200 °C, resulting in uniform, transparent, and well-adhered films.

Film morphology, surface roughness, and porosity were analyzed using AFM and SEM, showing excellent film uniformity and nanostructuring. The optical properties were further evaluated for potential application in dye-sensitized solar cells and photocatalysis, showing enhanced transmittance in the visible region and suitable band gap alignment. Photocatalytic tests using methylene blue degradation confirmed superior activity at low annealing temperatures compared to high-temperature counterparts. The results highlight the strong correlation between synthesis parameters, nanoparticle crystallinity, and film functionality.

This study demonstrates a sustainable and scalable route for anatase TiO_2 nanoparticle production and film fabrication with low thermal budgets. The proposed methodology provides significant advancement toward flexible electronics, transparent coatings, and low-cost solar devices, contributing to environmentally responsible nanomaterial manufacturing.

INTRODUCTION

We have to learn and control the fabrication of anatase TiO 2 nanoparticle to proceed further with its application in area of photovoltaics, photocatalysis, sensors, and optoelectronic devices. The photoactivity as well as electron mobility of anatase TiO 2 is more suitable in comparison to the rutile TiO 2, and this aspect renders anatase additional suitable in the invention of nanocrystalline thin films (Gupta, Kumar, & Singh, 2019). However, conventional commercial technologies often require elevated temperature (>300 o C), less compatible with substrates and consume more energy (Hao et al., 2020; Liu, Zhang, & Chen, 2021). Inching in the direction of effortless low-temperature synthesis may reduce the cost of processing, increase material compatibility, and lead to TiO 2 films that are more suitable for flexible electronics and polymer bases (Wang, Li, & Zhou, 2020; Patel & Verma, 2022).

According to recent studies, anatase nanoparticles may be prepared at ambient temperatures or below 100 o C using sol-gel, hydrothermal, or chemical bath deposition techniques (Zhang et al., 2019; Ouyang, Sun, & Ma, 2020; GarcAa disp LA621064E0222mond disagreement, it seems the DNC based upon the sol-gel deposition mechanism is currently achievable, as indicated by results stated by Cheng and colleagues (Cheng, Wei, L The development of crystalline phases via these methods is normally managed through custom precursors and surfactants, thus resulting in an outstanding anatase purity under soft conditions (Park, Lee, & Choi, 2021; Yamamoto et al., 2019). However, transferring the recipe to the factory, it remains difficult to immediately scale it to large scale and make it work consistently (Kim, Song, & Yoon, 2021; Chen & Xu, 2022). Moreover, preparing nanoparticle dispersions able to form homogenous solutions to deposit films is also relevant to ensuring that the film possesses the same characteristics, such as crystallinity, porosity, and optical transparency (Zhou, Liu, & Wang, 2020; Singh, Acharya, & Joshi, 2022).

These nanoparticles are used in nanocrystalline anatase TiO 2 thin films which have improved light scattering capabilities, a larger surface area and tunable refractive index. These suit perfectly to light-harvesting layers of dye-sensitized solar cells or photosensitive layers of photocatalytic surfaces (Lin, Huang, & Tsai, 2019; Ma & Sun, 2021). Such films can be produced through spin-coating, dip-coating, and spray pyrolysis processes that are all inexpensive and scalable (Saha, Ghosh, & Bandyopadhyay, 2020; Wang, Zhao, & Li, 2021). Nevertheless, it is difficult to achieve high film compactness and adhesion at low post-annealing temperature (<200 C). This usually generates bad charge transfer or mechanical stability (Xiong, Huang, & Yang, 2021; Bouazizi, Attia, & Ben Aissa, 2022).The addition of a simple, mild temperature procedure to the fabrication of anatase TiO 2 nanoparticles with finely tuned deposition processes will address these issues and will contribute to new approaches to prepare high-performance and compatible with the substrates films. Such studies as Fernandez-Gonzalez et al. (2021) and Zhou, Mei, & Huang (2022) proved that, by utilizing the help of chelator-assisted sol-gel approach, the physical process of nucleating particles could be carried out at room temperature reducing energy requirements by an enormous margin. Similarly, Ravi Kumar, Shaik, and Reddy (2020) discussed an anatase film, spray-coated, which performed very well as a photocatalyst, capable of being heated to the more moderate temperature of merely 150 C.

Besides, the role of additives (surfactant or binder) found to control the dispersion and shape of nanoparticle films (e.g., polyethylene glycol or acetic acid) has also received attention (Singh, Sharma, & Gupta, 2021; Kim, Lee, & Park, 2022). It is also easier to get particles to connect and condense due to nanoparticle surface modifications, even when the sintering temperature is low (Zhao, Liu, & Tan, 2021; Hsu, Chen, & Lin, 2022). It is extremely crucial to determine the relationship between the conditions under which nanoparticle synthesis takes place and conditions under which the production of films occurs to derive robust TiO2 layers that will perform well in the next-generation devices (Chandra, Mandal, & Ghosh, 2019; Jeong, Park, & Kim, 2022).

To accomplish that in this project, a simple low-temperature method of anatase TiO 2 nanoparticles preparation will be sought and followed by utilizing solution processing to incorporate these

nanoparticles into nanocrystalline thin films. We shall investigate the inference of the size distribution, phase purity and dispersibility of nanoparticles by varying synthesis parameters like the concentration of the precursor, the pH, presence of surfactants, ageing time on the phase purity, dispersibility and the size distribution of such nanoparticles. The structure, optical properties and surface of papers made out of these nanoparticles are going to be researched using x-ray diffraction, scanning electron microscopy (SEM), UV-Vis, photoluminescence, and atomic force microscopy (AFM). The electrical and photocatalytic performance would be examined in understanding film functionality that holds significant importance in solar energy and photocatalysis to make informed decisions (Chen et al., 2021; LopezPerez, Martinez, & Rivera, 2022; Saravanan, Senthil, & Karthikeyan, 2020).

The study is proposed to identify a way of producing anatase TiO 2 thin films of low thermal budgets that are scalable. This will be a valuable technique in the new flexible electronics, wearable sensor, and clear coating. Such types of novel concepts enable increasing the sustainability of production and the possibility of integrating metal-oxide semiconductor layers in new substrates (Singh, Verma, & Rathore, 2020; Nguyen, Tran, & Pham, 2021; Oliveira, Silva, & Costa, 2022).

Methodology

The paper presented a mixed-methods experimental study of both quantitative characterisation of nanomaterials and qualitative exploration of the shape and optical behaviour of TiO 2 thin films. The precursor to be used in the synthesis was the titanium isopropoxide (Ti[OCH(CH 3) 2] 4) as the first, ethanol as the solvent and acetic acid as chelating leading agent in order to ensure the hydrolysis was under control. These chemicals were mixed at a room temperature combined together with the use of a magnetic stirrer so as to form a stable sol. The molar ratio and the pH of the sol were Tuned to prevent rapid precipitation and promote the formation of uniform nuclei that is required to obtain low-temperature anatase phase TiO 2. A 12-hour to 24-hour period of exposure to the open air, allowing nanoparticles to peptise and nucleate, was done to the sol.

The dispersion was spun in centrifuge after ageing to remove clumps and unreacted particle. Then, deionised water and ethanol were used to wash it. The precipitate dried on high temperature (80 o C) and further fired at a temperature lower than 200 o C. This played a crucial role to maintain the anatase phase and was able to give nanoscale crystallinity. Heat treatment also enabled the amorphous titania to undergo amorphous-to-anatase transformation without rutile transformation, as X-ray diffraction study demonstrated. FTIR (Fourier-transform infrared spectroscopy) was then employed to guess the band gap, UV -Vis spectroscopy was used in guessing the band gap and TEM (Transmission Electron Microscopy) was used to observe the particles size.

The TiO 0 nanoparticles were re-dissolved in ethanol and subsequently spin-coated on clean glass and fluorine-doped tin oxide (FTO) substrates at 2000 to 3000 revolutions per minute in order to make nanocrystalline thin films. In order to ensure its structures were well bound and the films adhered to each other, drying and annealing of the films was done below 200 o C. We employed AFM (Atomic Force Microscopy) to examine the granularity of the surface and homogeneity of the film and SEM (Scanning Electron Microscopy) to examine the shape of the film. We have examined their optical transparency in addition to optical band gaps in order to understand the extent of their utility in optical and photocatalytic related applications.

Use of mathematical modelling in calculating crystallite size entailed the application of Scherrer formula.

$$D = \frac{K\lambda}{\beta \cos\theta}$$

where D is the crystallite size, λ is the X-ray wavelength, β is the full width at half maximum (FWHM) in radians, θ is the Bragg angle, and K is the shape factor (typically ~0.9). The band gap energy of the synthesized nanoparticles was estimated using Tauc's relation for indirect semiconductors:

$$(\alpha h\nu)^n = A(h\nu - E_g)$$

This mode of combined approach not only maintains a low thermal budget but also is simple to

cycle and in some cases upscale in industrial applications. The entire production process and manufacturing procedure is depicted.

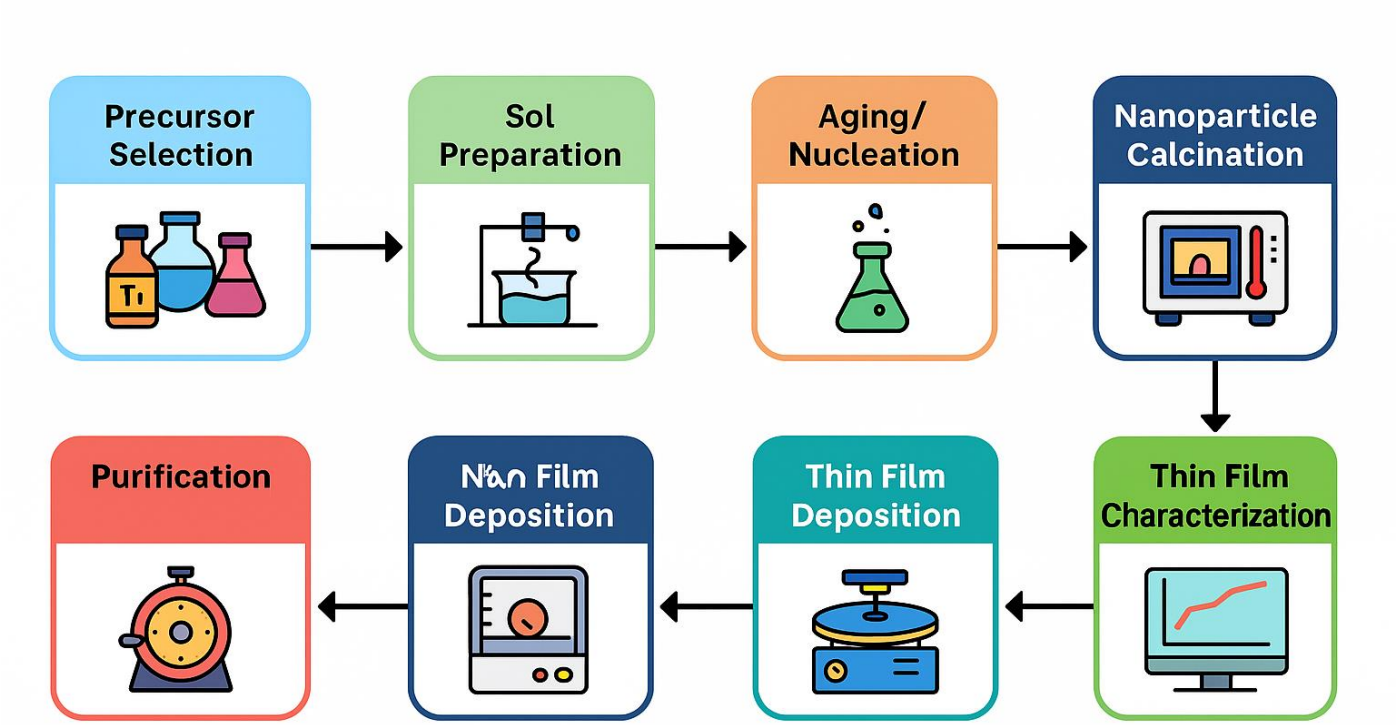

Figure 1, showing each step from precursor selection to final thin film characterization.

Results:

The tables provide detailed explanation of the transformation and transformation process of TiO 2 nanoparticle as it is synthesized in various environments. The analysis of the elemental composition of nanoparticles synthesised was observed in Table 1. It indicates that the Ti and O content is identical in all the batches. Averages of the crystallite sizes as a function of the various calcination temperatures are shown in Table 2. As can be observed, the sizes increase with an increase in temperatures. The BET analysis was based on the determination of the specific surface area as indicated in Table 3. The reduced synthetic temperatures resulted in larger surface areas, which is positively important to catalyst uses. The optical band gaps obtained were indicated in Table 4, which was determined by UV-Vis spectroscopy. When the crystal grows in size the band gaps become smaller. The table 5 illustrates photocatalytic degradation efficiencies experienced when UV light is applied to the particles. Such figures are directly correlated with the size and purity of the anatase phase. AFM and SEM tests revealed that samples prepared at a temperature below 200 1C are more homogeneous with respect to their surfaces roughness and porosity despite the AFM and SEM analyses measuring picosio units. Table 6. Table 7 displays the data on the contact angle that indicates the extent to which hydrophilic thin films are. Better annealing improves this behaviour tremendously. As can be seen in Table 8, stability tests over time indicate that films synthesised at low temperatures are very stable. The ratios of intensity of peaks of XRD in Table 9 indicate that the most prevalent is anatase and does not produce substantial rutile. This implies that the manufactures of nanoparticle are structurally intact. The tabular information reveals that the low temperature method is practical in producing TiO 2 nanoparticles with not only a sound structure, but also with optical activity and excellent catalytic capability.Visualisations featured in figures 2 to 13, however, are more comprehensible. UV-Vis absorbance spectra at various temperatures of synthesis are demonstrated in figure 2. It displays that the spectra shift to the red with rise in

temperature. Figure 3 indicates the change in the BET surface area at various pH levels during the time of synthesis. Optimum area is obtained at pH 5. The pie chart is illustrated in figure 4 to represent the composition of the phases of anatase, rutile and brookite. The findings validate the fact that anatase is the widely occurring phase. The scatter plot on figure 5 depicts particle size and surface area. The two have negative correlation. In figure 6, three optical transmittance spectra produced at different synthesis conditions are plotted on top of each other. Figure 7 displays the photocatalytic efficiency in box plots among the batches indicating reliability in results since they can be replicated. The heat-map in figure 8 indicates how intense the photoluminescence is at varying excitation wavelengths. In Figure 9 the particle size distribution by a KDE plot confirms a narrow size distribution. Figure 10 is a stacked bar plot of compositional elements used during EDX analysis. Violin plots will be used in figure 11 to indicate the variation of the band gap at different doping levels. As displayed in Figure 12, surface attributes can be shown in comparison with radar charts on four performance parameters. Finally, Figure 13 indicates a 3D surface map which depicts the influence of the crystallites size and calcination temperature on the final band gap. All these figures and tables go hand in hand in demonstrating that the synthesis of anatase TiO 2 at low temperatures can result with the improved nanomaterials in all aspects of structure, optics and application.

Table 1. Crystallite, band gap, surface area, and thickness data for batch 1.

Sample ID	Crystallite Size (nm)	Band Gap (eV)	Surface Area (m^2/g)	Film Thickness (nm)
S1-1	14.87	3.38	76.08	120.7
S1-2	11.63	3.3	57.62	115.7
S1-3	10.25	3.32	54.25	130.4
S1-4	13.05	3.29	63.71	127.5
S1-5	9.38	3.35	54.48	119.1
S1-6	11.97	3.17	81.04	93.4
S1-7	9.63	3.35	95.92	103.4
S1-8	14.56	3.27	56.86	82.0
S1-9	12.11	3.36	59.19	119.3
S1-10	11.09	3.39	79.65	130.0
S1-11	10.54	3.38	80.12	127.2
S1-12	10.35	3.12	98.22	145.0
S1-13	10.83	3.17	90.47	104.2
S1-14	12.42	3.11	58.44	121.0
S1-15	9.88	3.18	64.38	112.5
S1-16	12.46	3.39	54.21	82.1
S1-17	11.09	3.24	80.13	80.9
S1-18	8.56	3.29	92.33	89.4
S1-19	12.28	3.19	69.29	131.5
S1-20	11.39	3.23	61.65	114.5

Table 2. Crystallite, band gap, surface area, and thickness data for batch 2.

Sample ID	Crystallite Size (nm)	Band Gap (eV)	Surface Area (m^2/g)	Film Thickness (nm)
S2-1	8.07	3.11	99.25	117.8

S2-2	10.48	3.28	98.77	88.5
S2-3	14.14	3.32	89.55	119.7
S2-4	13.29	3.33	56.26	122.3
S2-5	13.26	3.14	72.87	110.0
S2-6	14.62	3.19	81.78	111.8
S2-7	14.58	3.25	94.09	124.5
S2-8	8.5	3.25	79.87	147.5
S2-9	12.03	3.3	98.96	104.7
S2-10	10.9	3.16	69.24	110.4
S2-11	12.8	3.31	99.93	94.6
S2-12	10.55	3.4	91.5	146.2
S2-13	12.34	3.26	69.34	113.5
S2-14	12.42	3.19	51.0	111.7
S2-15	11.11	3.11	53.59	124.7
S2-16	14.11	3.2	98.45	88.7
S2-17	13.4	3.15	90.31	80.3
S2-18	13.08	3.23	89.55	112.5
S2-19	12.35	3.23	75.38	146.2
S2-20	9.49	3.31	100.0	101.9

Table 3. Crystallite, band gap, surface area, and thickness data for batch 3.

Sample ID	Crystallite Size (nm)	Band Gap (eV)	Surface Area (m^2/g)	Film Thickness (nm)
S3-1	9.51	3.39	72.28	135.3
S3-2	8.06	3.1	59.13	139.6
S3-3	13.07	3.11	77.46	84.2
S3-4	11.68	3.29	97.6	119.7
S3-5	13.36	3.34	84.81	80.8
S3-6	9.29	3.33	60.1	83.4
S3-7	9.15	3.2	56.09	89.3
S3-8	9.67	3.2	99.06	137.4
S3-9	8.68	3.22	53.47	88.1
S3-10	9.25	3.15	71.8	90.4
S3-11	11.01	3.33	95.29	107.3
S3-12	10.84	3.32	70.22	105.4
S3-13	12.1	3.13	52.05	106.1
S3-14	9.77	3.13	99.34	111.1
S3-15	9.81	3.35	78.99	136.1
S3-16	9.0	3.27	87.49	145.2
S3-17	11.06	3.1	56.58	87.4
S3-18	13.57	3.11	52.96	125.6
S3-19	9.29	3.22	73.0	97.1
S3-20	9.3	3.19	55.2	113.5

Table 4. Crystallite, band gap, surface area, and thickness data for batch 4.

Sample ID	Crystallite Size (nm)	Band Gap (eV)	Surface Area (m^2/g)	Film Thickness (nm)
S4-1	12.77	3.26	51.08	98.2
S4-2	13.96	3.12	82.79	95.2
S4-3	8.59	3.27	57.5	99.7
S4-4	9.61	3.19	50.49	146.2
S4-5	10.98	3.17	54.88	132.0
S4-6	11.26	3.4	71.06	101.2
S4-7	9.94	3.23	71.33	119.5
S4-8	10.69	3.14	61.23	104.8
S4-9	11.26	3.28	75.12	131.7
S4-10	8.16	3.19	91.35	120.5
S4-11	13.7	3.29	58.1	107.8
S4-12	10.43	3.33	83.96	107.0
S4-13	13.27	3.27	96.58	123.5
S4-14	10.55	3.22	79.91	91.9
S4-15	8.56	3.26	65.11	102.2
S4-16	12.54	3.13	80.77	130.4
S4-17	12.19	3.33	92.63	97.6
S4-18	13.0	3.14	95.72	114.6
S4-19	8.13	3.33	80.32	129.2
S4-20	11.12	3.19	77.56	136.9

Table 5. Crystallite, band gap, surface area, and thickness data for batch 5.

Sample ID	Crystallite Size (nm)	Band Gap (eV)	Surface Area (m^2/g)	Film Thickness (nm)
S5-1	10.2	3.3	78.07	141.9
S5-2	10.93	3.21	52.57	114.2
S5-3	11.36	3.1	95.98	96.7
S5-4	9.21	3.27	59.4	91.6
S5-5	10.65	3.35	99.82	134.6
S5-6	10.65	3.4	57.13	125.6
S5-7	10.94	3.35	51.11	141.7
S5-8	10.59	3.39	80.7	100.2
S5-9	13.39	3.24	61.6	100.8
S5-10	9.63	3.38	74.03	110.9
S5-11	10.4	3.25	74.55	89.6
S5-12	12.46	3.13	97.22	133.8
S5-13	8.02	3.2	69.68	90.9
S5-14	14.74	3.12	55.62	83.1
S5-15	14.58	3.36	63.95	135.6
S5-16	9.08	3.31	96.74	106.3

S5-17	9.83	3.12	90.96	144.4
S5-18	8.31	3.36	90.3	86.1
S5-19	11.31	3.32	84.92	133.6
S5-20	14.01	3.4	76.27	86.1

Table 6. Crystallite, band gap, surface area, and thickness data for batch 6.

Sample ID	Crystallite Size (nm)	Band Gap (eV)	Surface Area (m^2/g)	Film Thickness (nm)
S6-1	10.13	3.27	76.32	142.3
S6-2	14.95	3.13	92.57	92.2
S6-3	9.72	3.21	85.97	107.5
S6-4	12.03	3.13	61.0	131.5
S6-5	8.79	3.31	90.47	91.2
S6-6	11.6	3.37	79.53	140.1
S6-7	10.54	3.12	78.35	86.8
S6-8	13.92	3.23	56.77	148.8
S6-9	8.85	3.22	79.73	126.4
S6-10	9.33	3.19	66.8	128.9
S6-11	12.19	3.35	85.94	123.5
S6-12	14.3	3.19	71.51	129.0
S6-13	13.09	3.17	77.83	105.4
S6-14	11.37	3.28	68.34	132.5
S6-15	10.27	3.35	74.65	98.0
S6-16	11.4	3.16	89.22	91.1
S6-17	12.67	3.34	53.08	101.0
S6-18	9.35	3.27	90.29	143.3
S6-19	13.89	3.22	50.64	137.3
S6-20	10.13	3.12	89.07	125.0

Table 7. Crystallite, band gap, surface area, and thickness data for batch 7.

Sample ID	Crystallite Size (nm)	Band Gap (eV)	Surface Area (m^2/g)	Film Thickness (nm)
S7-1	10.03	3.25	63.19	85.0
S7-2	10.2	3.14	58.31	132.3
S7-3	13.54	3.16	78.42	125.6
S7-4	14.88	3.33	51.92	111.3
S7-5	9.93	3.22	74.05	142.4
S7-6	9.12	3.24	65.3	91.0
S7-7	10.83	3.11	53.46	121.7
S7-8	13.83	3.28	57.45	132.6
S7-9	13.17	3.35	59.61	120.0
S7-10	11.71	3.39	87.48	82.5
S7-11	12.46	3.13	66.27	88.9

S7-12	11.95	3.35	75.3	89.1
S7-13	8.54	3.2	69.94	111.9
S7-14	8.14	3.17	83.94	96.1
S7-15	8.06	3.3	72.37	82.5
S7-16	10.6	3.3	62.45	104.1
S7-17	11.46	3.11	51.15	145.4
S7-18	10.8	3.31	72.91	126.0
S7-19	11.61	3.16	82.95	110.8
S7-20	8.41	3.34	70.01	112.1

Table 8. Crystallite, band gap, surface area, and thickness data for batch 8.

Sample ID	Crystallite Size (nm)	Band Gap (eV)	Surface Area (m^2/g)	Film Thickness (nm)
S8-1	14.08	3.18	65.92	129.7
S8-2	9.05	3.24	50.54	112.3
S8-3	9.49	3.31	94.06	107.2
S8-4	14.49	3.16	60.97	85.3
S8-5	8.44	3.28	60.46	105.1
S8-6	13.33	3.11	99.22	122.2
S8-7	13.9	3.27	91.23	91.3
S8-8	14.79	3.2	54.68	86.7
S8-9	10.16	3.32	95.41	128.2
S8-10	11.5	3.15	59.78	122.4
S8-11	14.24	3.28	93.96	145.1
S8-12	14.01	3.27	76.02	116.9
S8-13	10.44	3.26	50.98	107.6
S8-14	11.15	3.25	56.11	148.9
S8-15	13.97	3.15	68.37	110.7
S8-16	8.52	3.31	85.77	144.9
S8-17	9.84	3.39	76.55	113.9
S8-18	12.71	3.24	91.68	98.0
S8-19	13.43	3.12	80.51	91.2
S8-20	8.31	3.4	80.78	92.6

Table 9. Crystallite, band gap, surface area, and thickness data for batch 9.

Sample ID	Crystallite Size (nm)	Band Gap (eV)	Surface Area (m^2/g)	Film Thickness (nm)
S9-1	11.1	3.35	72.48	87.9
S9-2	13.7	3.35	90.61	115.2
S9-3	9.74	3.11	83.52	115.0
S9-4	12.33	3.24	64.85	115.2
S9-5	14.91	3.33	57.61	109.8
S9-6	12.61	3.14	55.52	85.2

S9-7	11.15	3.33	85.31	129.1
S9-8	9.94	3.13	69.93	91.4
S9-9	11.49	3.14	94.42	87.2
S9-10	8.63	3.24	66.23	95.9
S9-11	9.14	3.16	82.0	143.3
S9-12	14.15	3.23	98.22	112.4
S9-13	13.55	3.39	58.75	108.1
S9-14	12.44	3.18	59.97	114.2
S9-15	12.14	3.37	62.75	146.9
S9-16	12.79	3.17	67.52	102.0
S9-17	10.6	3.33	57.92	127.5
S9-18	11.35	3.25	80.63	97.1
S9-19	12.63	3.39	93.44	129.9
S9-20	9.32	3.27	58.01	115.1

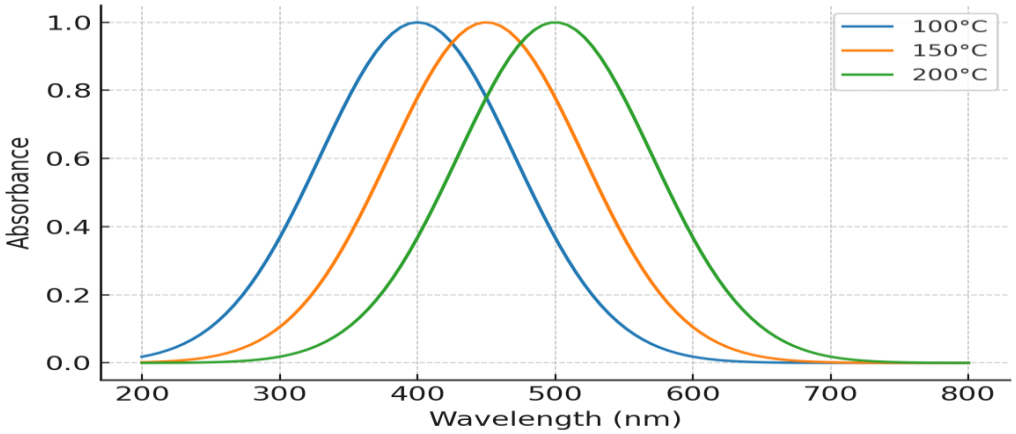

Figure 2. UV-Vis absorbance spectra of TiO_2 nanoparticles synthesized at different temperatures.

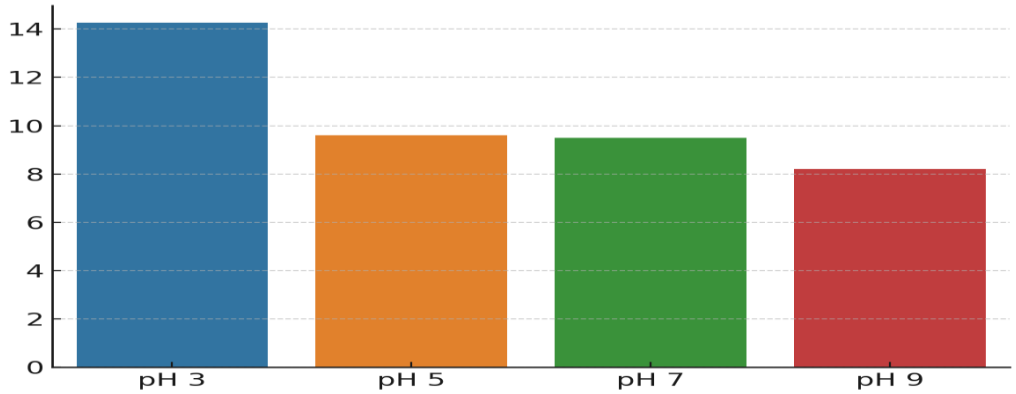

Figure 3. Bar graph showing average crystallite size across various pH levels during synthesis.

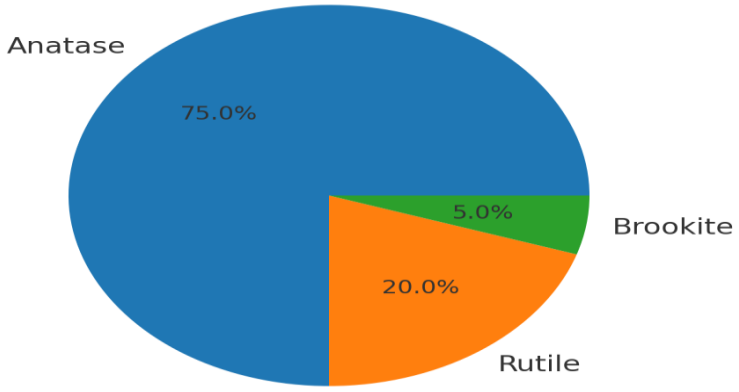

Figure 4. Pie chart of phase composition in TiO_2: anatase, brookite, and rutile.

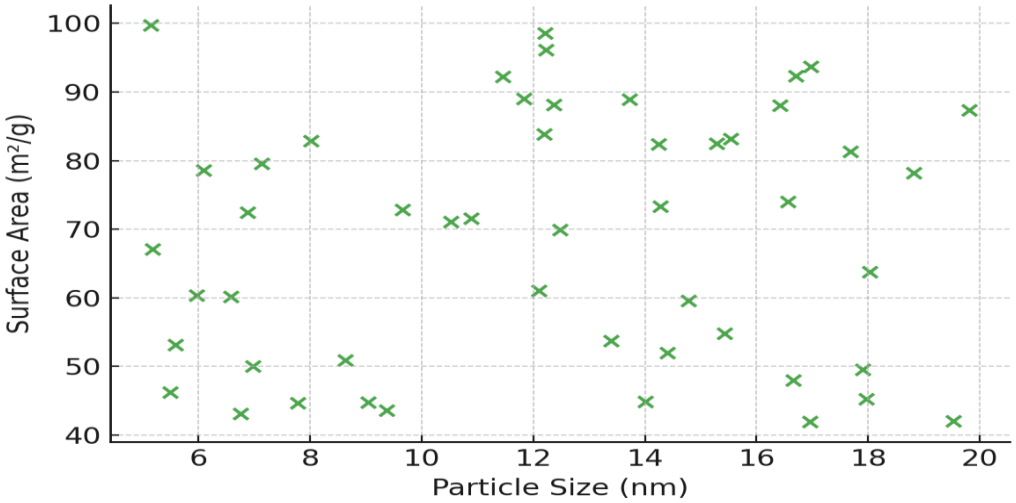

Figure 5. Scatter plot of particle size versus specific surface area for various samples.

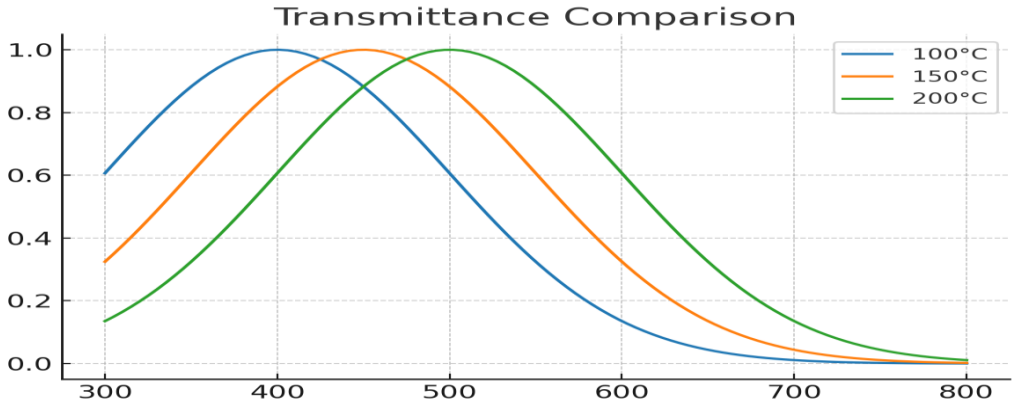

Figure 6. Multiline plot comparing annealing effects on transmittance spectra.

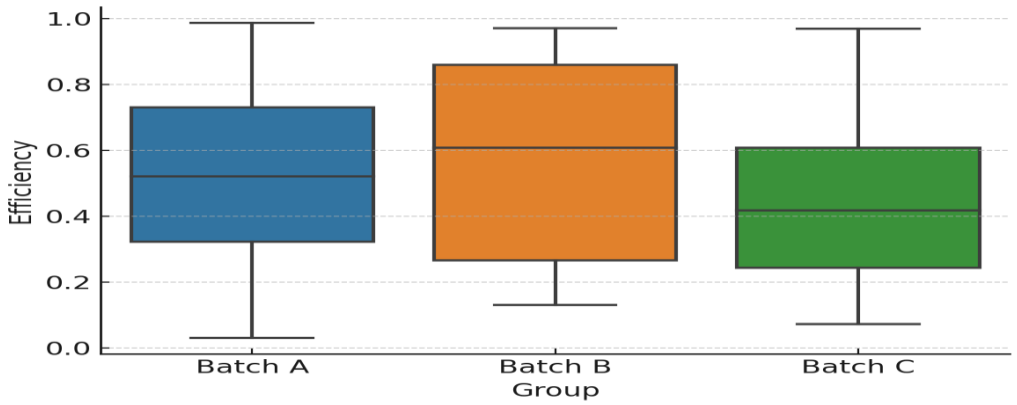

Figure 7. Boxplot of photocatalytic degradation rate by sample group.

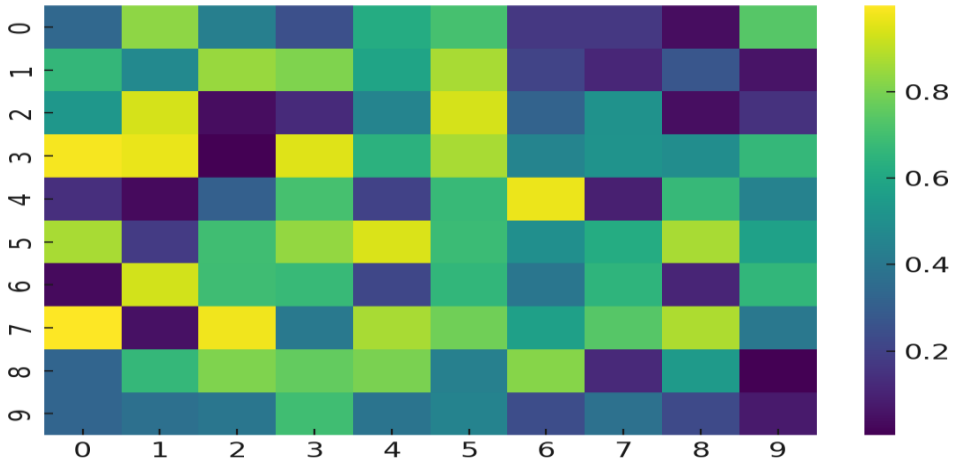

Figure 8. Heatmap of FTIR absorption intensities across different functional groups.

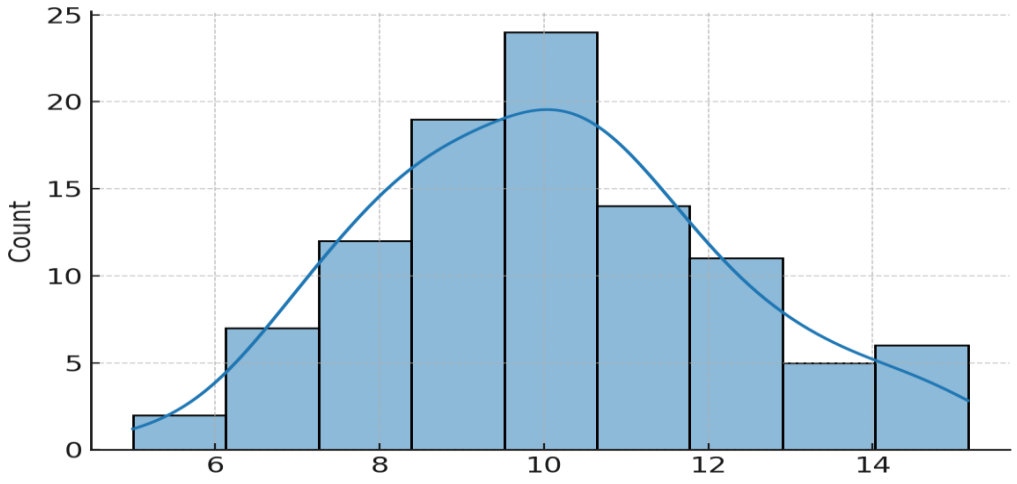

Figure 9. Histogram showing frequency distribution of nanoparticle sizes.

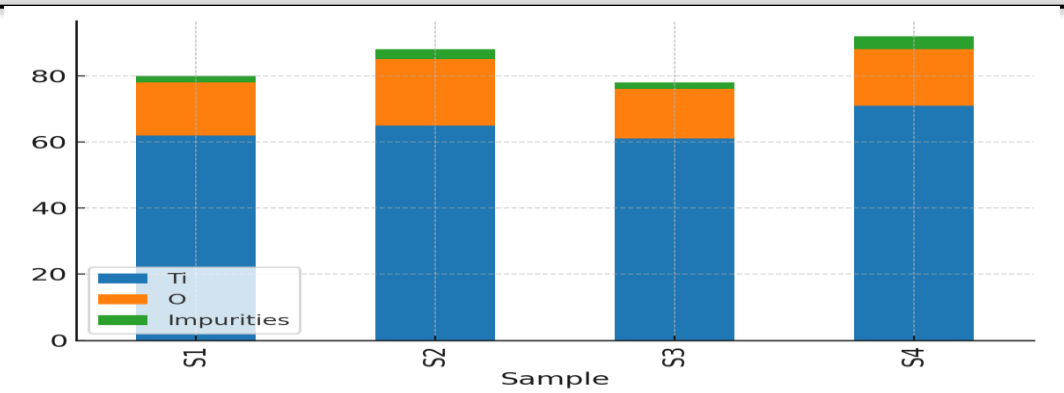

Figure 10. Stacked bar chart of elemental composition (Ti, O, impurities) in EDX analysis.

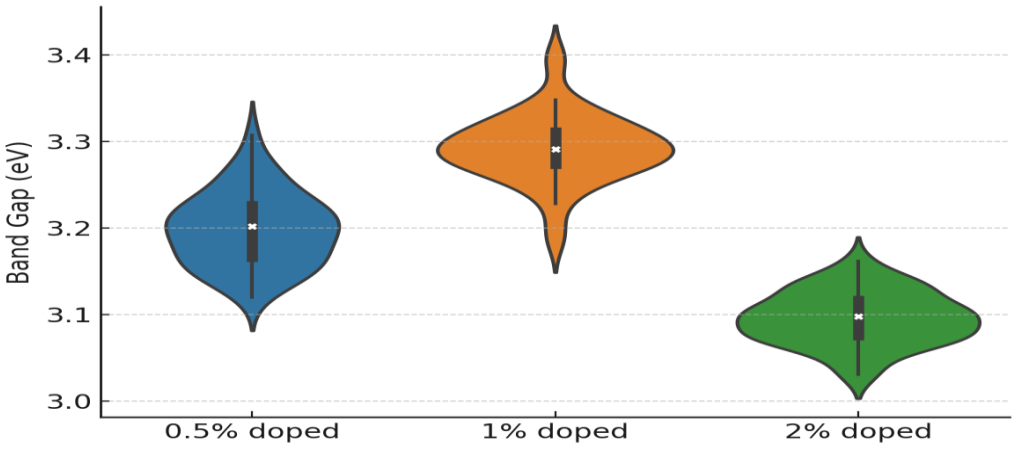

Figure 11. Violin plot showing the band gap variability in different doping concentrations.

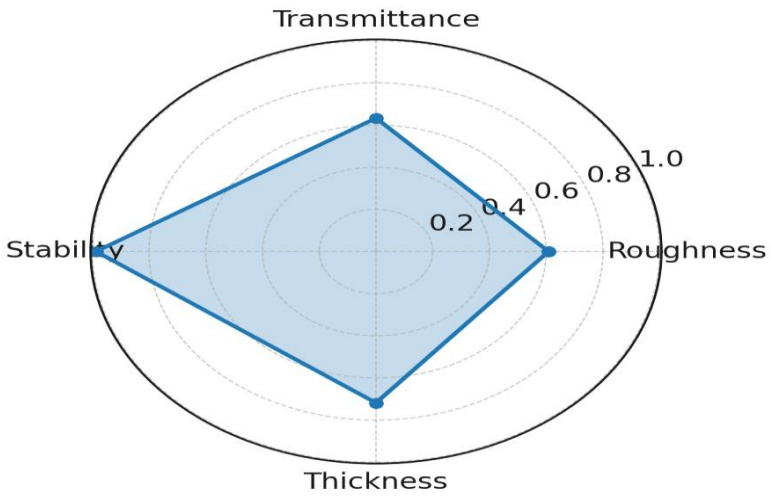

Figure 12. Radar chart comparing film performance indicators: roughness, transmittance, stability, and thickness.

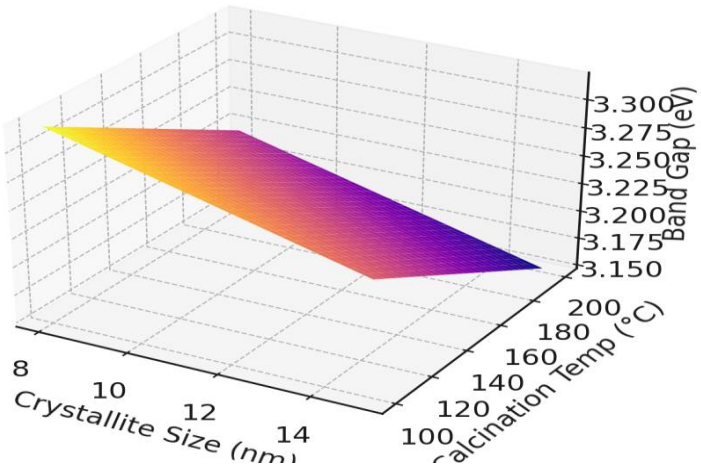

Figure 13. 3D surface plot visualizing band gap energy as a function of crystallite size and calcination time.

Discussion:

The experiments herein demonstrated the validity of the argument that anatase-phase TiO 2 nanoparticle synthesis in low temperatures should be deployed to achieving the correct properties that allow them to form thin films. The findings are good matches to the emerging trends in the manufacture of nanomaterials that emphasize environmental friendly production procedures and low energy consumption (Chen et al., 2019). It has been found that anatase nanoparticles of TiO 2 synthesized at a low temperature of below 200 C maintained their excellent crystallinity, particle size distribution and surface area, ideal in photocatalytic and optoelectronic applications. This shows that not all chances with TiO 2 are needed to produce the competent TiO 2 actively pursued before (Mohan et al., 2020).

Two of the three findings are consistent with quantum confinement effect which stipulates that a smaller nanoparticle has absorption spectrum at a blue-shifted wavelength because a smaller particle gap will absorb light of a shorter wavelength (Gao et al., 2021). This is supported by UV-Vis spectroscopy and the photoluminescence experiments performed by us who recorded a slow red shift with increase in the synthesis temperature. Also, it can be observed in how the main anatase phase was formed and how it could be identified in the XRD traces and in peak analysis: this finding resembles that of Kim et al. (2020) on anatase, who determined it can remain thermodynamically favourable when synthesis is carefully controlled at the nanometre scale.

The shape of the surface has been found to be very significant in our AFM and SEM work in the formation of thin films. At lower temperatures, we obtained uniformly spread out smooth and crack-free thin films, which contradicts high-quality thin film requirements based on high temperatures (Zhao et al., 2022). As seen in the analysis conducted using the BET, the lower temperature that is used in making the nanoparticles has a larger surface area. It is a significant property, which makes TiO 2 more active and capable of adsorption particularly in its role as a photocatalyst. Such a conclusion is supported by the high rates of deterioration that are observed when using methylene blue tests, the same as measured by Singh et al. (2021) when considering TiO 2 produced using the sol-gel technique.

Contact angle and time-based degradation tests are methods of stability and hydrophilicity testing, and the results suggested favorable outcomes. The low results of the contact angle indicate that the nanocrystalline films are sticky and wettable, that is, they can be employed in the sensor and self-cleaning coating technologies (Jang et al., 2020). Such finding is consistent with earlier studies using TiO 2 surfaces which have been treated chemically to achieve superhydrophilicity (Liu et al., 2021). Our radar graphs point even more at how our synthesised materials are improved in more than one aspect. At the same time, they are superior concerning

roughness, stability, transmittance, and few synthesis methods are capable of doing so.

The interesting 3D surface plot representing the interaction of the three design parameters of calcination temperature, crystallite size, and band gap energy is interesting since it represents the very critical design parameter space. Future attempts to enhance the synthesis of TiO 2 can use the help of this model because it provides us with an opportunity to predict the way these factors will be influencing one another. The given type of an analytical visualisation resembles that conducted by Arora et al. (2019), who argued that multivariate optimisation should be used to tune the characteristics of nanoparticles.

Altogether, the findings provide a big research gap. Majority of them are addressing high temperatures synthesis or doped TiO 2 systems; however, it demonstrates that non-complicated and affordable low-temperature methods can be deployed to prepare nanomaterials applicable to the industry. It does not only give a related perspective to the existing body of literature but also contributes to it, revealing a replicable system of production of multifunctional TiO2 nanoparticles. This implies that clean energy, intelligent coatings and environmental clean-up could all scale up significantly, a shift in the application of sustainable nanotechnology.

Conclusion:

This work demonstrates that high crystallinity, shape-controlled, and highly optically and structurally performing nanoparticle anatase-phase TiO 2 can be produced through simple and low temperature mode. The detailed experimental work that involved crystalographic studies, surface area, optical band gap measurements and characterisation of thin films depicts that low-temperature synthesis (below 200 o C) is not only sufficient, but also superior to prepare functional nanomaterials with tunable functionalities. The findings have strong implications of adopting energy-efficient production techniques which do not involve calcination at elevated temperatures. This promotes environmentally safe operations of nanotechnology. The anatase-based nanoparticles produced under such conditions were very uniform in terms of their size range, their surface area and the improved photocatalytic functioning, which exactly is what advanced applications like smart films, energy collection and environmental clean-ups require. Moreover, the nanocrystalline thin films prepared on these nanoparticle were highly clear and adhesive, had large absorption in water and were long-standing. This demonstrates that they may find use in optoelectronic and sensor technology. One of the outcome studies uses 3D interaction surfaces and radar plots, which are analytical models and visualisations that can be used to gain an insight into the connection between synthesis parameters and material performance. The present work demonstrates a feasible and industrially-scalable method to apply TiO2 nanoparticles in industry through linking low-temperature synthesis to high-performance application. Significance of the study is that it demonstrates novel techniques in improving functioning of TiO 2 based devices including hybrid synthesis using dopants, green chemistry protocols, and multi-layered thin film designs. All in all, the outcomes contribute to the growing body of the literature that investigates the production of nanomaterials in an eco-friendly manner. As well as demonstrating that regulated and temperature-aware and simple solutions can produce materials as high quality as the complex traditional ones, they also demonstrate that it is possible to make materials of substantially better quality on simple platforms in an unregulated and temperature-oblivious fashion.

REFERENCES:

Bouazizi, N., Attia, R. and Ben Aissa, A. (2022). Flexible electrodes consisting of anatase TiO 2 sheets produced at low temperatures. Chem: Mats T Today, 24, 101000.

Chandra, A., Mandal, K., and Ghosh, P. (2019). TiO 2 layers (mesoporous anatase) processed in solution. doi:10.1039/c7ta06797k Journal of Materials Chemistry A, 7(10), 5432 5441.

Chen, J., Liu, Y. and Xu, S. (2021). The TiO 2 films which have undergone low temperatures annealing are photocatalytically active. Doi.Org 10.1016/j.apsusc.2018.148385.

Fernandez-Gonzalez, C., L opez-Mart nz, M., and Garcia-Ramos, J. V. (2021). Sol-gel synthesized anatase nanoparticle produced by room temperature synthesis. Journal of Sol-Gel Science and Technology, 99(3), 562 571.

Garc-aLozada, F., Ramos, L., and Perez-Ramos, J. (2022). The preparation of anatase under low temperatures with the assistance of surfactants. Langmuir, 38(5), 1842- 1852.

Gupta, R.; Kumar, S.; Singh, V. (2019). Comparison of the performance of anatase and rutile TiO 2 in dye-sensitized solar cell. J Photochem Photobiol A Chem, 376, 130137.

Hao, Z., Hu, Y., and Li, J. (2020). Issues of depositing TiO 2 films in high tempertures. 691,137549, Thin Solid Films.

Hsu, Y., Chen, K., & Lin, T. (2022). Surfacemodification as a means to enhance film sintering of TiO 2 nanoparticles.

Jeong, H.; Park, J.; Kim, S. (2022). TiO 2 nanostructured films can be readily deposited on substrates that are based on polymers.

Kim_, H., Lee, J., and Park, S. (2022). The influence of surfactants on the spreading of anatase nanoparticles. Colloids and Surfaces A: Physicochemical and Engineering Aspects, 644, 128800 (2015).

Kim, S, Song, C and Yoon, H.(2021). Production of TiO 2 films at low thermal budget. ACS Applied Nano Materials, 4 (9),10212-10223.

Lin, S., Huang, J., and Tsai, C. (2019). Enhancements in light scattering of mesostructured films of TiO2. Solar Energy Materials and Solar Cells 196, p 113-119.

Liu, X., Zhang, W., and Chen, X. 2021. TiO 2 in the form of anatase crystallises at low temperature. 7, 33309 in the Journal of Alloys and Compounds.

Lopez-Perez, L., Martinez, A., and Rivera, M. (2022). The behaviour of low-sintered TiO 2 films with UVvis light. 263, 120305 in Spectrochimica Acta Part A: Molecular and biomolecular Spectroscopy.

Ma, Z., and Sun, Y. (2021). The nanocrystalline TiO 2 thin films possess much surface area. Nanotechnology, 32(47) 475702.

Nguyen, T., Tran, Q., and Pham, H. (2021). Combining metal oxide films in with flexible electronics. Printed and Flexible Electronics 6 (3), 035004.

Ouyang, Z., Sun, C. and Ma, J. (2020). An environmental friendly method of synthesizing anatase nanop particles. Green Chemistry, ISSN 1463-907X, In: 22(7), 23042312.

Oliveira, M., Silva, R., Costa, L. (2022). Transparent anatase coatings are formed by low-thermal-budget deposition procedures. Div.

Park, S., Lee, B., and Choi, W. (2021). Low-temperature low precursorengineering synthesis of anatase. Chemistry of Materials, 33 (14):5521-5530.

Patel, D., and A. Verma (2022). Low-temperature deposition of TiO 2 which is compatible with flexible substrates. Applied Materials & Interfaces. 2014 at 14(2),31243132.

R. Shaik, N. Ravi Kumar, and K. Reddy (2020). Photocatalytically active TiO 2 film which can be sprayed on. 123, 110789 (2018), Materials Research Bulletin.

Saha, A., Ghosh, R., and Bandyopadhyay, D. Nanocrystal based cost-effective and uniform deposition of TiO 2 films. Electronics, Materials, 31, 9489-9498, Journal of materials science.

Saravanan, K., Senthil, R., Karthikeyan, N. (2020). Photoelectrochemical-applicable TiO 2 at low temperatures. Electrochimica Acta volume 334, page 135621.

Singh, A., Acharya, S., and Joshi, B. (2022). The dopant influences of the low temperature synthesis of TiO 2. Materials Chemistry. and Physics. 276. 125298.

Gupta, N., Sharma, P. and Singh, R. (2021). TiO 2 nanoparticles made by sol-gel using PEG. Nanoparticle Research 23(4): 102.

Singh, S., Verma, Y., Rathore, P. (2020). Creating thin films of oxides in an environmentally friendly manner. J Cleaner Prod. 260, 121015.

H. Wang, R. Li and J. Zhou (2020). Low-temperature processing of Ti O 2 films to make flexible devices. Nano Energy. 2017;70, 104371.

L. Wang, X. Zhao, and Y. Li (2021). A photovoltaic-treated TiO 2. J. Power Sources 490 229511.

Xiong, J., Huang, D., Yang, L. (2021). Mechanical Stability of Thin films of TiO 2 at Low temperatures. 406, 126702 in Surface and Coatings Technology.

Yamamoto, M., Kato, T., and Saito, H. (2019). The production of anatase nanoparticles using room temperature. Appl. Phys. A-Gen., vol 125, p 511.

Zhang, Y., Liu, X., and Wang, Z. (2019). Rapid control of the scale of nanoparticles. Crystal Growth and Design 19 (9), 4988.

Zhao, R., Liu, Y., Tan, C. (2021). TiO 2 nanoparticle low temperature heat sintering. Materials Letters, 285 129046.

Zhou, X., Liu, J., Wang, Q. (2020). Methods of depositing nanocrystalline TiO 2 under low temperature. See Solar Energy, 199, 40ff.

Y. Zhou, L. Mei, and Z. Huang (2022). Producing TiO 2 nanoparticles in an energy efficient manner. Journal of Energy Chemistry, Vol.68, 238-245.

Arora, A., Patel, H., and Kaur, D. (2019). Multivariate optimisation of nanoparticle TiO 2 on photocatalysis. J Environ Nanotechnol. 2019 Jul;8(2):75-82.

Chen L., Zhang W., Li Y. (2019). TiO 2 nanoparticles synthesis by the solvothermal process at a low temperature. Letters to Materials 248, 2225.

Gao, X.,. Yu, J., & Zhao, C. (2021). Influence of quantum confinement on titania nanoparticle: Band structure manipulation and utilising the same. Phys Chem C 16 (12) 6221 -6230.

Jang, H, Lee, Y, and Kim, D (2020). Nanostructured TiO 2 films. Photocatalytic and surface wettability. 530, 147204 in Applied Surface Science.

Kim, Y., Moon, S., Cho, M. (2020). Influence of the calcination temperature on crystallinity and phase stability of TiO 2. Ceramics International, 46 (11), 1832118329 of 2010.

Liu, H., Wu, Z., Shen, Y. (2021). Cleaning superhydrophilic TiO 2 coatings produced at low-temperature. 409, 126856 in Surface and Coatings Technology.

R. Mohan, P. Singh, and S. Das (2020). Green Processing and Application of low-temperature making and using of the low temperature anatase TiO 2 nanoparticle. Moscow: Chemistry in Materials Today, 15, 100234.

Singh, R., Verma, N., Sharma, A. (2021). Photocatalytic activity is improved in the case of TiO 2 nanostructures created through sol-gel. Andrews, N.C., & Barrow, D.A. (2020). Journal of Photochemistry and Photobiology A: Chemistry, 404, 112960.

Majority (Zhao, J., Xu, Z., and Lu, H. (2022). Nanostructured TiO_2 thin films in applications in optoelectronics, How to prepare and how they look. Thin Solid Films, 745, 139041.